11518 *Inorg. Chem.* **2009**, *48*, 11518–11524
DOI: 10.1021/ic900784t

Inorganic Chemistry
Article

Syntheses, Crystal and Electronic Structures, and Physical Properties of Two Quaternary Chalcogenides: $La_4FeSb_2Q_{10}$ (Q = S, Se)

Hua-Jun Zhao,[†,‡] Long-Hua Li,[†,‡] Li-Ming Wu,[†] and Ling Chen*[,†]

[†]*Key Laboratory of Optoelectronic Materials Chemistry and Physics, Fujian Institute of Research on the Structure of Matter, Chinese Academy of Sciences, Fuzhou, Fujian 350002, People's Republic of China, and* [‡]*Graduate School of the Chinese Academy of Sciences, Beijing 100039, People's Republic of China*

Received April 24, 2009

Two new quaternary chalcogenides, $La_4FeSb_2S_{10}$ and $La_4FeSb_2Se_{10}$, have been synthesized from the stoichiometric mixture of elements by solid-state reactions at 1100 °C. The compounds crystallize in the orthorhombic space group *Pbcm* with a = 15.066(4) Å, b = 7.590(2) Å, c = 13.341(4) Å, and Z = 4 and a = 15.596(5) Å, b = 7.869(2) Å, c = 13.960(4) Å, and Z = 4, respectively. These structures represent an unique three-dimensional network, in which SbQ_3 trigonal pyramids (Sb−S < 2.60 Å, Sb−Se < 2.80 Å) are connected via a relatively weak Sb−Q bond (Sb−S ≈ 2.90 Å, Sb−Se ≈ 3.00 Å) in a novel teeter-totter $(SbQ_4)_n$ chain motif. The theoretical studies confirm the Sb−Q bonding interactions within such teeter-totter chains. Their optical band gaps are measured to be 1.00 and 0.85 eV. At room temperature, their electrical conductivities are about 10^{-4} S/cm. Both compounds display antiferromagnetic interactions between Fe centers, and their effective magnetic moments are 5.25 and 6.17 μ_B, respectively.

Introduction

Binary or multinary antimony chalcogenides are interesting because of their potential application as thermoelectric materials.[1−4] For example Sb_2Te_3,[1] $Ag_{1-x}Pb_{18}SbTe_{20}$,[2] $Mo_3Sb_5Te_2$,[3] and $AgSb_xBi_{3-x}S_5$[4] show promising thermoelectric properties. The structural chemistry of ternary or quaternary Sb/Q/M compounds (Q = chalcogenides, M = transition metal or main group metal) is impressive partly owing to the diverse local coordination environments around Sb, for example, trigonal pyramid, incomplete octahedra (with two vacant equatorial sites), square pyramid, and distorted octahedron. However, rare earth-antimony-chalcogenides are less studied, several ternary compounds are known as $La_7Sb_9S_{24}$,[5] $EuSbSe_3$,[6] Tm_2SbTe,[7] $CeSbTe$,[8] and only a few quaternary $K_2Ln_{2-x}Sb_{4+x}Se_{12}$,[9] $K_2Ln_2Sb_2Se_9$,[10] and $Na_9Gd_5Sb_8S_{26}$[11] are reported. Among them, $La_7Sb_9S_{24}$ has been attempted as a thermoelectric compound, and unfortunately, its band gap is too wide.[5] On the other hand, the quaternary A/Ln/Sb/Q (A = alkali metal, Ln = lanthanide) chalcogenides exhibit even wider energy gap because of the strong ionic bonding interactions between the cationic A and the anionic Sb/Q framework.[9−11] A possible way to reduce the band gaps of quaternary A/Ln/Sb/Q compounds is to partially or totally replace A with the less electropositive metals.[4] Thus, we chose Fe as a fourth component in the quaternary Ln/Sb/Q/TM (Ln = lanthanide, Q = chalcogenides, TM = transition metal) system, which has not been investigated before. Up to now, only two iron antimony sulfides are known as $FePb_4Sb_6S_{14}$[12,13] and $FeSb_2S_4$,[14] no ternary or quaternary iron antimony selenide is reported. In this paper, we report the synthesis, crystal and electronic structure, and physical properties of the first quaternary $La_4FeSb_2Q_{10}$ (Q = S, Se).

*To whom correspondence should be addressed. E-mail: chenl@fjirsm.ac.cn. Phone: (011)86-591-83704947.

(1) Thonhauser, T.; Scheidemantel, T. J.; Sofo, J. O.; Badding, J. V.; Mahan, G. D. *Phys. Rev. B* **2003**, *68*, 085201–085208.
(2) Hsu, K.-F.; Loo, S.; Guo, F.; Chen, W.; Dyck, J. S.; Uher, C.; Hogan, T.; Polychroniadis, E. K.; Kanatzidis, M. G. *Science* **2004**, *303*, 818–821.
(3) Dashjav, E.; Szczepenowska, A.; Kleinke, H. *J. Mater. Chem.* **2002**, *12*, 345–349.
(4) Kim, J.-H.; Chung, D.-Y.; Bilc, D.; Loo, S.; Short, J.; Mahanti, S. D.; Hogan, T.; Kanatzidis, M. G. *Chem. Mater.* **2005**, *17*, 3606–3614.
(5) Assoud, A.; Kleinke, K. M.; Kleinke, H. *Chem. Mater.* **2006**, *18*, 1041–1046.
(6) Jin, G.; Crerar, S. J.; Mar, A.; Albrecht-Schmitt, T. E. *J. Solid State Chem.* **2006**, *179*, 1595–1600.
(7) Abdusalyamova, M. N.; Chuiko, A. G.; Golubkov, A. Yu.; Popov, S. I.; Parfenova, L. S.; Prokofiev, A.; Smirnov, I. A. *J. Alloys Compd.* **1994**, *205*, 107–109.
(8) Wang, Y. C.; Poduska, K. M.; Hoffmann, R.; Disalvo, F. J. *J. Alloys Compd.* **2001**, *314*, 132–139.
(9) Chen, J. H.; Dorhout, P. K. *J. Alloys Compd.* **1997**, *249*, 199–205.
(10) Choi, K. -S.; Hanko, J. A.; Kanatzidis, M. G. *J. Solid State Chem.* **1999**, *147*, 309–319.
(11) Park, S.; Kim, S.-J. *J. Solid State Chem.* **2001**, *161*, 129–134.
(12) Matsushita, Y.; Ueda, Y. *Inorg. Chem.* **2003**, *42*, 7830–7838.
(13) Léone, P.; Le Leuch, L. M.; Palvadeau, P.; Molinié, P.; Moëlo, Y. *Solid State Sci.* **2003**, *5*, 771–776.
(14) Lukaszewicz, K.; Pietraszko, A.; Stepień-Damm, J.; Kajokas, A.; Grigas, J.; Drulis, H. *J. Solid State Chem.* **2001**, *162*, 79–83.

Published on Web 11/17/2009

Experimental Section

Synthesis. The elements were used as acquired and stored in a nitrogen-filled glovebox (moisture and oxygen level is less than 0.1 ppm), and all manipulations were performed inside the glovebox. The La (99.99%) was purchased from Huhhot Jinrui Rare Earth Co. Ltd. The Fe (99.98%), S (99.999%), and Se (99.999%) were purchased from Alfa Aesar China (Tianjin) Co. Ltd. The Sb (99.99%) was purchased from Sinopharm Chemical Reagent Co., Ltd. All reactants in evacuated fused-silicon tubes were placed in resistance furnaces with controlled temperature.

$La_4FeSb_2S_{10}$. The first synthesis attempt started from elements with 1:1:1 ratios according to the nominal binaries FeS/La_2S_3/Sb_2S_3. Elements of La, Fe, Sb, and S were weighed accordingly (that is in a ratio of La/Fe/Sb/S = 2:1:2:7) with a overall loading of about 300 mg and loaded into a quartz tube, which was evacuated and sealed. The sample was heated to 1100 °C in 36 h and kept for 48 h, subsequently cooled (3 °C/h) to 200 °C before the furnace was turned off. Good quality single crystals were obtained. However, the X-ray diffraction (XRD) patterns indicated a mixture of an unknown phase and a known ternary $FeSb_2S_4$. The single crystal diffraction data of a prismatic crystal in black color yielded a refined formula of $La_4FeSb_2S_{10}$ (nominal $1FeS:2La_2S_3:1Sb_2S_3$). The EDX results confirmed the presence of La, Fe, Sb, and S in a molar ratio about 4:1:2:10. No other element, such as Si from the reaction container, was found. After the structure establishment, the title quaternary sulfide was synthesized from an elemental mixture of La, Fe, Sb, S in the ratio of 4:1:2:10. The heating profile was the same as mentioned above, and homogeneous black target product was obtained as indicated by the XRD pattern shown in Figure 1a.

$La_4FeSb_2Se_{10}$. The synthesis of the quaternary selenide analogue is nearly a parallel reaction. Similar reactions as that for sulfide were loaded except for Se were used instead, and the heating profile was optimized as follows: heating to 1100 °C in 36 h and keeping for 10 h, (shorter in comparison with that of sulfide) subsequently cooling at 30 °C/h to 600 °C (higher in comparison with that of sulfide), and annealing at this temperature for 393 h (not necessary for the sulfide analogue) before shutting down the furnace. The homogeneity of the black sample was confirmed by the XRD pattern as shown in Figure 1b. But such process did not generate good quality single crystals, which can only be obtained by slowly cooling (3 °C/h) the stoichiometric mixture of Fe, La, Sb, Se elements from 1100 to 300 °C. However, this pathway produced La_3Se_4 as an impurity as well.

No obvious corrosion on the quartz jacket was observed in any case. The two compounds are both stable in air for about 1 year.

Crystal Structure Determinations. Data collections were performed on a Rigaku Saturn70 CCD equipped with graphite-monochromated Mo Kα radiation ($\lambda = 0.71073$ Å) at 293 K. The data were corrected for Lorentz and polarization factors. Absorption corrections were performed. All structure were solved by the direct methods and refined by the full-matrix least-squares fitting on F^2 by SHELX-97.[16] For $La_4FeSb_2S_{10}$ all atoms were refined with anisotropic thermal parameters. Unfortunately, the present technique did not generate $La_4FeSb_2Se_{10}$ single crystals with good quality. Comparatively, the single crystal size of $La_4FeSb_2Se_{10}$ is smaller than that of $La_4FeSb_2S_{10}$, for example, 0.07 × 0.05× 0.03 versus 0.09 × 0.07× 0.06 mm^3, and the diffraction intensities of the selenide are much weaker than those of the sulfide, for example, the mean (I/σ) is 7.45 for $La_4FeSb_2Se_{10}$ versus 16.83 for $La_4FeSb_2S_{10}$. We had tried absorption corrections by both multiscan method[15] and numerical absorption correction for $La_4FeSb_2Se_{10}$. After the numerical absorption correction, the first refinement cycle generated three non-positive definite Se4, Se5, and Se6 atoms. The following refinement cycle with these three Se atoms with isotropic thermal parameters generated a very high residual peak of 16.07 e $Å^{-3}$ near the Se6 site within a distance of 0.54 Å. This poor result might be related to the small size of the crystal (0.07 × 0.05 × 0.03 mm^3) and the absorption coefficient mu × midsize = 34.89 × 0.05 = 1.74. Therefore, the numerical absorption correction did not generate good results in this case. On the other hand, we had also collected the diffraction data at 123 K on the same crystal. The equivalent isotropic displacement parameters of Se2, Se4, Se5, and Se6 did not display an obvious temperature dependence, and the equivalent isotropic displacement parameters of other atoms showed an obvious decrease of approximately 54% (as average) when the temperature decreased from 293 to 123 K; however, the ADP of Se4, Se5, and Se6 were still non-positive definite. Such unchangeable non-positive definite character may be caused by the relative low diffraction intensities of the $La_4FeSb_2Se_{10}$ crystal. The R_1/wR_2 ($I > 2\sigma(I)$) values at 123 K were 0.1350/0.3687, respectively, and the highest residual peak was 22.16 e $Å^{-3}$ within a distance of 0.63 Å to Se6 atom. Therefore, the low temperature data did not generate better refinement results in this case either. The crystallographic data reported here were collected at 293 K, corrected with multiscan absorption corrections, and all atoms except Se1 and Se3 refined with anisotropic thermal parameters. The refinement converged at acceptable values, R_1/wR_2 ($I > 2\sigma(I)$) values of 0.1040/0.2454, and highest residual peak of 6.53 e $Å^{-3}$ within a distance of 0.75 Å to the

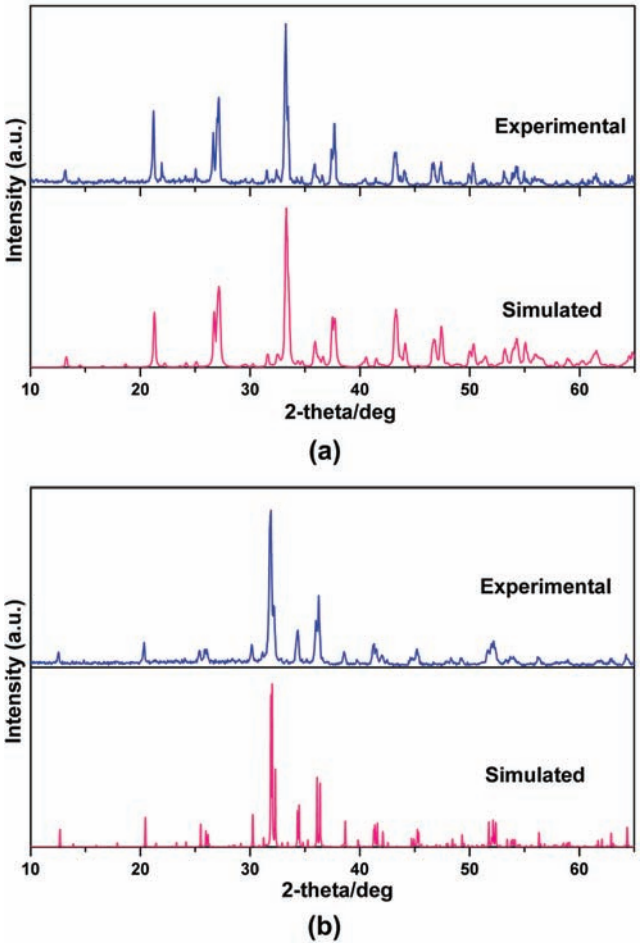

Figure 1. Experimental and simulated X-ray powder diffraction patterns of (a) $La_4FeSb_2S_{10}$ and (b) $La_4FeSb_2Se_{10}$.

(15) *CrystalClear*, version 1.3.5; Rigaku Corp.: The Woodlands, TX, 1999.
(16) Sheldrick, G. M. *SHELXTL*, version 5.1; Bruker-AXS: Madison, WI, 1998.

Table 1. Crystallographic Data and Refinement Details for $La_4FeSb_2S_{10}$ and $La_4FeSb_2Se_{10}$

	$La_4FeSb_2S_{10}$	$La_4FeSb_2Se_{10}$
fw	1175.59	1644.49
crystal system	orthorhombic	orthorhombic
crystal color	black	black
Z	4	4
space group	*Pbcm* (No. 57)	*Pbcm* (No. 57)
a (Å)	15.066(4)	15.596(5)
b (Å)	7.590(2)	7.869(2)
c (Å)	13.341(4)	13.960(4)
α (deg.)	90.00	90.00
β (deg.)	90.00	90.00
γ (deg.)	90.00	90.00
V (Å^3)	1525.56(7)	1713.2(9)
F(000)	2064	2783
D_c (g cm^{-3})	5.119	6.376
M (mm^{-1})	16.689	34.888
$2\theta_{max}$ (deg.)	54.96	54.96
GOF on F^2	1.075	1.138
R_1, wR_2 ($I > 2\sigma(I)$)[a]	0.0174, 0.0409	0.1040, 0.2454
R_1, wR_2 (all data)	0.0247, 0.0435	0.1139, 0.2496
largest difference peak and hole (e Å^{-3})	0.841 (0.93 Å from La1), −1.704 (0.01 Å from La3)	6.528 (0.75 Å from La3), −7.163 (0.65 Å from Se6)

[a] $R_1 = \sum||F_o| - |F_c||/\sum|F_o|$, $wR_2 = [\sum w(F_o^2 - F_c^2)^2/\sum w(F_o^2)^2]^{1/2}$.

Table 2. Atomic Coordinates and Equivalent Isotropic Displacement Parameters of $La_4FeSb_2S_{10}$[a]

atom	Wyckoff	x	y	z	U(eq)
La1	*4d*	0.06284(2)	0.37696(4)	0.25	0.00745(8)
La2	*4d*	0.31030(2)	0.62060(4)	0.25	0.00749(8)
La3	*4c*	0.37737(2)	0.25	0	0.01097(8)
La4	*4c*	0.87305(2)	0.25	0	0.01117(8)
Sb1	*4d*	0.21584(2)	0.04881(4)	0.25	0.01008(9)
Sb2	*4d*	0.53544(2)	0.45490(4)	0.25	0.01008(9)
Fe1	*4c*	0.12437(5)	0.25	0	0.0091(2)
S1	*8e*	0.54356(6)	0.0775(1)	0.10472(7)	0.0091(2)
S2	*4d*	0.3751(1)	0.2397(2)	0.25	0.0164(3)
S3	*8e*	0.03534(6)	0.0863(1)	0.10488(7)	0.0095(2)
S4	*8e*	0.70823(6)	0.4158(1)	0.10522(7)	0.0097(2)
S5	*8e*	0.21027(7)	0.4238(1)	0.10239(7)	0.0090(2)
S6	*4d*	0.1267(1)	0.7597(2)	0.25	0.0163(3)

[a] U_{eq} is defined as one third of the trace of the orthogonalized U_{ij} tensor.

La3 atom. Crystallographic data and structural refinement details are summarized in Table 1, the positional coordinates and isotropic equivalent thermal parameters are given in Tables 2 and 3, and some important bond distances are listed in Table 4. More details of the crystallographic data are given in the Supporting Information.

X-ray Powder Diffraction. The XRD patterns were collected on a Rigaku DMAX 2500 diffractometer. The measured XRD patterns (Figure 1) are in good agreement with the calculated ones, which also approve the symmetry refined by the single crystal diffraction data.

Elemental Analysis. The elemental analyses of La, Fe, Sb, S and Se have been examined with the aid of a field emission scanning electron microscope (FESEM, JSM6700F) equipped with an energy dispersive X-ray spectroscope (EDX, Oxford INCA).

Electronic Structure Calculations. Electronic structure calculations were performed using the self-consistent full-potential linearized plane wave method (LAPW)[17] within density functional theory (DFT)[18] and the local density approximation (LDA) for the exchange correlation energy with the aid of the WIEN2k program. We have used the LDA+U approach[19] with the SIC method for double counting correction,[20] as implemented in the WIEN2k program. A value of 5.71 eV was used for the effective Hubbard U ($J = 0$). The electronic configurations for La, Sb, Fe, S, and Se are as follows: La, [Xe]5p^{1}6s^2; Sb, [Kr]4d^{10}5s^{2}5p^3; Fe, [Ar]3d^{6}4s^2; Se, [Ar]3d^{10}4s^{2}4p^4; S, [Ne]3s^{2}3p^4. The values of the atomic radii were taken to be 2.50 au for La, 2.31 au for Sb, 2.29 au for Fe, 2.13 au for Se and 2.03 au for S. Convergence of the self-consistent iterations was performed for 16 k points inside the irreducible Brillouin zone to within

Table 3. Atomic Coordinates and Equivalent Isotropic Displacement Parameters of $La_4FeSb_2Se_{10}$[a]

atom	Wyckoff	x	y	z	U(eq)/U(iso)*
La1	*4d*	0.064601(4)	0.370990(8)	0.25	0.00951(1)
La2	*4d*	0.687980(4)	0.126180(8)	0.25	0.00947(1)
La3	*4c*	0.379151(4)	0.25	0	0.01323(1)
La4	*4c*	0.876431(4)	0.25	0	0.01575(1)
Sb1	*4d*	0.215810(5)	0.04931(1)	0.25	0.01377(2)
Sb2	*4d*	0.533979(5)	0.450731(9)	0.25	0.01167(2)
Fe1	*4c*	0.12359(1)	0.25	0	0.01210(3)
Se1	*8e*	0.544389(5)	0.081302(9)	0.102851(5)	0.01165(1) *
Se2	*4d*	0.370840(7)	0.24386(2)	0.2500	0.02397(3)
Se3	*8e*	0.034840(5)	0.08237(1)	0.106062(5)	0.01243(1) *
Se4	*8e*	0.706959(5)	0.416412(9)	0.102579(6)	0.01195(2)
Se5	*8e*	0.211529(4)	0.424410(9)	0.102680(5)	0.01128(2)
Se6	*4d*	0.129350(7)	0.75792(2)	0.25	0.02514(3)

[a] U_{eq} is defined as one third of the trace of the orthogonalized U_{ij} tensor. Values marked in asterisks refer to U(iso).

Table 4. Selected Bond Lengths (Å) of $La_4FeSb_2S_{10}$ and $La_4FeSb_2Se_{10}$

	$La_4FeSb_2S_{10}$	$La_4FeSb_2Se_{10}$
La1-Q3 × 2	2.909(1)	3.0347(5)
La1-Q3 × 2	2.965(1)	3.0678(6)
La1-Q5 × 2	2.990(1)	3.1076(7)
La1-Q6	2.990(2)	3.1530(9)
La1-Q6	3.060(2)	3.2078(8)
La2-Q5 × 2	2.896(1)	3.0343(5)
La2-Q1 × 2	2.952(1)	3.0593(7)
La2-Q6	2.962(2)	3.0317(9)
La2-Q4 × 2	2.971(1)	3.0885(6)
La2-Q2	3.052(2)	3.1453(8)
La3-Q1 × 2	3.091(1)	3.2062(6)
La3-Q1 × 2	3.153(1)	3.2350(7)
La3-Q5 × 2	3.154(1)	3.2821(7)
La3-Q4 × 2	3.174(1)	3.2779(6)
La3-Q2 × 2	3.337(1)	3.493(1)
La4-Q3 × 2	3.080(1)	3.1680(7)
La4-Q5 × 2	3.095(1)	3.2405(6)
La4-Q4 × 2	3.118(1)	3.2789(7)
La4-Q3 × 2	3.222(1)	3.3087(6)
La4-Q6 × 2	3.337(1)	3.492(1)
Sb1-Q4 × 2	2.462(1)	2.6038(5)
Sb1-Q6	2.574(2)	2.6600(6)
Sb1-Q2	2.802(2)	2.8618(7)
Sb2-Q1 × 2	2.458(1)	2.6018(5)
Sb2-Q2	2.549(2)	2.7430(6)
Sb2-Q2	2.918(2)	3.0205(7)
Fe1-Q5 × 2	2.298(1)	2.4124(4)
Fe1-Q3 × 2	2.303(1)	2.4182(4)

(17) Singh, D. *Planewawes, Pseudopotentials, and the LAPW Method*; Kluwer Academic: Boston, MA, 1994.

(18) (a) Hohenberg, P.; Kohn, W. *Phys. ReV.* **1964**, *136*, B864–B871. (b) Kohn, W.; Sham, L. *Phys. Rev.* **1965**, *140*, A1133–A1138.

(19) Anisimov, V. I.; Aryasetiawan, F.; Lichtenstein, A. I. *J. Phys.: Condens. Matter* **1997**, *9*, 767–808.

(20) Anisimov, V. I.; Solovyev, I. V.; Korotin, M. A.; Czyzyk, M. T.; Sawatzky, G. A. *Phys. Rev. B* **1993**, *48*, 16929–16934.

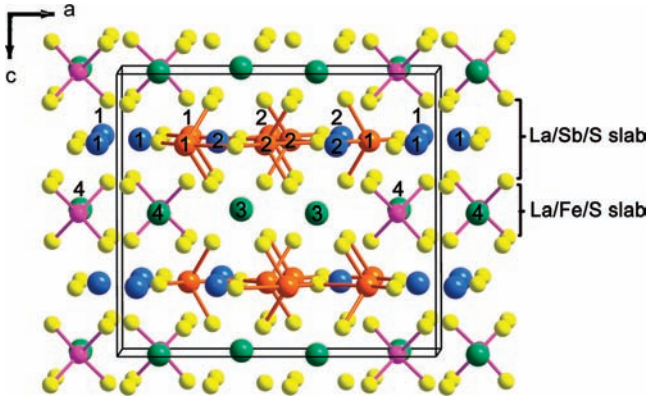

Figure 2. View approximately along the *b* axis of $La_4FeSb_2S_{10}$. Light blue, La1 and La2; Light green, La3 and La4; Orange, Sb; Pink, Fe; Yellow, S. La−S bonds are omitted for clarity. Sb−S bonds < 3.00 Å; Fe−S bonds < 2.40 Å.

0.0001 Ry with a cutoff −6.5 Ry between the valence and the core states. To analyze the degree of the bonding interaction between Sb and S, the integrated COHP (ICOHP; COHP = crystal orbital Hamilton populations)[21,22] values were calculated by the self-consistent tight-bonding first principles LMTO method (LMTO = linear muffin tin orbitals).[23,24]

Magnetic Susceptibility. The direct current (dc) magnetic susceptibility measurements were performed on a Quantum Design PPMS-9T magnetometer for the $La_4FeSb_2S_{10}$ and MPMS-XL magnetometer for the $La_4FeSb_2Se_{10}$ in the temperature range of 2−300 K. The X-ray pure polycrystalline samples were ground to fine powders to minimize the possible anisotropic effects and loaded into a gelatin capsule. The data were corrected for the susceptibility of the container and for the diamagnetic contribution from the ion core.

UV/vis Diffuse Reflectance Spectroscopy. The optical diffuse reflectance spectrum of powdery samples were measured at room temperature using a Perkin-Elmer Lambda 900 UV−vis spectrophotometer equipped with an integrating sphere attachment and $BaSO_4$ as a reference. The absorption spectrum was calculated from the reflection spectrum via the Kubelka-Munk function: $\alpha/S = (1 - R)^2/2R$, in which α is the absorption coefficient, *S* is the scattering coefficient, and *R* is the reflectance.[25]

Electrical Conductivity. The sample was thoroughly ground and then cold pressed into a circular pellet of $\Phi 6 \times 1$ mm^3, and the silver paint was used to create the electric contacts in the two opposite sides of pellet. The alternating current (ac) electrical resistance was measured in the frequency from 20 Hz to 1 MHz using a LCR4284A impedance analyzer with signal level of 1.0 V.

Results and Discussion

Crystal Structure. The structures of $La_4FeSb_2S_{10}$ and $La_4FeSb_2Se_{10}$ feature a new structure type. The projection of $La_4FeSb_2S_{10}$ is shown in Figure 2 as an example with all La−S bonds omitted for clarity. The detailed view of the La/Sb/S and La/Fe/S slabs are shown in Figure 3 and 4, respectively. The unique teeter-totter $(SbS_4)_n$ chains, as shown in Figure 3, are made of SbS_3 trigonal pyramids (Sb−S < 2.60 Å) that are connected via a relatively weak Sb−S interaction ≈ 2.90 Å (see coordination spheres in the Supporting Information). These chains are interconnected by $La1S_8$ and $La2S_8$ in a layered motif that parallels the *ab* plane, namely, the La/Sb/S slab (Figure 3). Between these La/Sb/S slabs, there are La3, La4 cations and FeS_4 tetrahedra that are arranged in a layered motif (namely, the La/Fe/S slab) as shown in Figure 4. The adjacent La/Sb/S and La/Fe/S slabs are further connected by LaS_8 and LaS_{10} polyhedra (Supporting Information) via the shared S−S edges and apexes. The formula of the title compounds can be written as $La_4[(FeS_4)(SbS_3)_2]$.

There are two crystallographically independent Sb atoms. Each Sb atom has three short and one long Sb−S bonds (Supporting Information), in the normal range of the Sb−S bonds. The three short Sb−S bonds with an

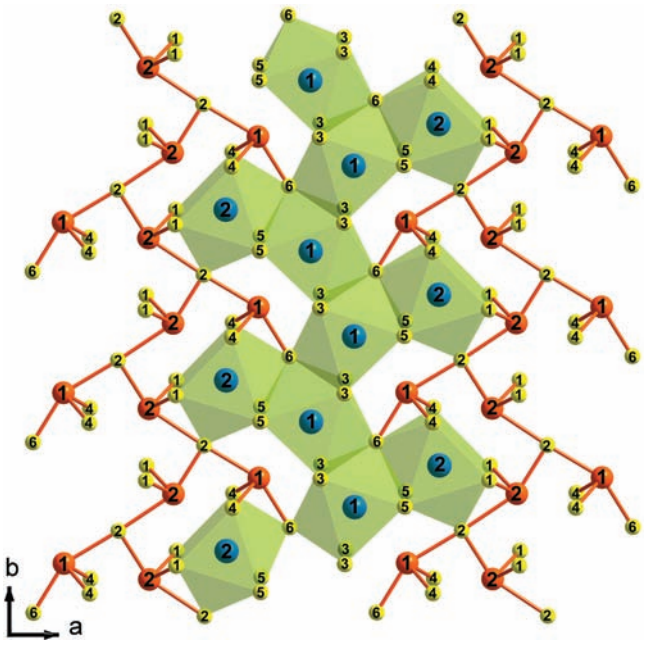

Figure 3. La/Sb/S slab viewed approximately along the *c* axis, in which the teeter-totter $(SbS_4)_n$ chains are interconnected by $La1S_8$ and $La2S_8$ polyhedra. Light blue, La1 and La2; Orange, Sb; Yellow, S. La−S bonds < 3.20 Å; Sb−S bonds < 3.00 Å.

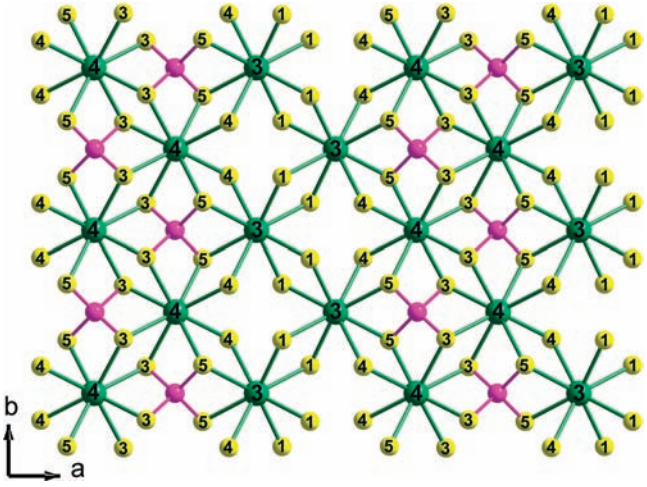

Figure 4. La/Fe/S slab perpendicular to the *c* axis. Light green, La3 and La4; Pink, Fe; Yellow, S. La−S bonds < 3.30 Å; Fe−S bonds < 2.40 Å.

(21) Dronskowski, R.; Blochl, P. E. *J. Phys. Chem.* **1993**, *97*, 8617–8624.
(22) Landrum, G. A.; Dronskowski, R. *Angew. Chem., Int. Ed.* **2000**, *39*, 1560–1585.
(23) Andersen, O. K. *Phys. Rev. B* **1975**, *12*, 3060–3083.
(24) Skriver, H. L. *The LMTO Method*; Springer: Berlin, Germany, 1984.
(25) Kortüm, G. *Reflectance Spectroscopy*; Springer-Verlag: New York, 1969.

Table 5. Selected Interatomic Distance (Å) and −ICOHP (eV/bond) Values for Sb−S

bond	interatomic distance	−ICOHP
Sb1−S4 × 2	2.46	2.540
Sb1−S6	2.57	1.457
Sb1−S2	2.80	0.751
Sb1−S3 × 2	3.35	0.028
Sb1−S5 × 2	3.46	0.012
Sb2−S1 × 2	2.46	2.576
Sb2−S2	2.55	1.528
Sb2−S2	2.92	0.308
Sb2−S4 × 2	3.26	0.0005
Sb2−S1 × 2	3.46	0.025

average of 2.50 Å generate a trigonal pyramid geometry, which is similar to that observed in $Sr_6Sb_6S_{17}$, in which the SbS_3 trigonal pyramid forms a Sb_3S_7 trimer via sharing corners.[26] The relatively long Sb1−S2 = 2.80 Å, Sb2−S2 = 2.92 Å bonds connect such trigonal pyramid into a teeter-totter chain as indicated by orange lines in Figure 3. Inclusion of these long bonds makes the local coordination of the Sb atom an incomplete octahedron (with two vacant equatorial sites), which has also been observed in $CrSbSe_3$,[27] in which the four Sb−Se bonds are 2.64, 2.64, 2.67, and 3.14 Å, respectively. Additionally, the Sb1 atom in $La_7Sb_9S_{24}$[5] also has three short Sb−S bonds of 2.5 Å and one long Sb−S bond of 2.83 Å. In $La_4FeSb_2Se_{10}$ reported here, the average 2.65 Å of the three short Sb−Se bonds and the long Sb−Se bond of 2.94 Å are naturally slightly longer than the corresponding Sb−S bonds in $La_4FeSb_2S_{10}$, but comparable to those in $CrSbSe_3$.[27] As indicated by the dashed lines in the Supporting Information, the distance between Sb and the four second nearest neighboring S atoms ranges from 3.26 to 3.46 Å, which is much longer than the average Sb−S bond distance of 2.74 Å within the teeter-totter chain. Our calculations revealed that these longer contacts are really weak interactions (see below Table 5).

Both La1 and La2 exhibit a normal bicapped trigonal prismatic coordination sphere with eight La−S bonds between 2.90 and 3.06 Å as detailed in the Supporting Information. Differently, the other two crystallographically independent La sites, La3 and La4 with La−S contacts in the range of 3.08 to 3.34 Å have approximate bicapped square antiprismatic environments. All these La−S distances are comparable to the normal range as in the related lanthanide chalcogenides, for example, La−S = 2.93 Å in γ-La_2S_3,[28] 2.91 Å in α-La_2S_3,[29] and 2.83 Å in $La_7Sb_9S_{24}$.[5] In case of $La_4FeSb_2Se_{10}$, the La−Se bond lengths range from 2.97 to 3.24 Å for La1/2 and 3.09 to 3.49 Å for La3/4. These value are very close to those in $La_3CuSnSe_7$ (3.10 Å as average).[30]

The Fe atom is tetrahedrally coordinated by S atoms with an average Fe−S distance of 2.30 Å and Fe−S−Fe angles ranging from 106.06° to 111.43°, such geometry is common in iron chalcogenides. For example, Fe−S = 2.34 Å in Fe_2SnS_4,[31] and 2.36 Å in Cu_2FeSnS_4.[32] The isolated FeS_4 tetrahedra are interconnected by La(3)/(4) polyhedra in a layered motif, namely, La/Fe/S slab, as shown in Figure 4. Such layered arrangement is similar as the Ba/Fe/S layer in $BaLa_2FeS_5$,[33] with only half of the Fe sites occupied. The mean Fe−Se = 2.41 Å distance in $La_4FeSb_2Se_{10}$ is consistent with the 2.42 Å distance in $BaFe_2Se_3$.[34]

Magnetic Properties. The susceptibility data were fit by the least-squares method to the Curie−Weiss equation $\chi_M = C/(T - \theta)$,where χ_M is the magnetic susceptibility, C is the Curie constant, and θ is the Weiss constant. The effective magnetic moment (μ_{eff}) was calculated from the equation $\mu_{eff} = (7.997C)^{1/2}\,\mu_B$.[35] The $La_4FeSb_2S_{10}$ obeys the Curie−Weiss law at high temperature with deviations below 16 K (Supporting Information). The parameters obtained from fitting are as follows: Curie constant, C = 3.45 emu K/mol; Weiss temperature, $\theta = -51.79$ K. The negative θ value suggests that significant antiferromagnetic interactions exist between the magnetic Fe ions (the nearest distance between Fe ions is 5.33 Å). The effective magnetic moment is 5.25 μ_B, which suggests that Fe(II) takes the high-spin state ($t_{2g}^4e_g^2$, $S = 2$), and this value is slightly higher than the "spin-only" moment (4.90 μ_B) calculated for a high-spin Fe(II).[36] Such a result is similar to that in $BaLa_2FeS_5$[33] (5.41 μ_B) in which the ground state Fe(II) has an unquenched orbital moment. The $La_4FeSb_2Se_{10}$ obeys the Curie−Weiss law at high temperature with deviations below 50 K (Supporting Information). The linear fit of the magnetic data in the range of 50−300 K gave a Curie constant of 4.76 emu K/mol and a Weiss constant of −103.67 K, which indicate that significant antiferromagnetic interactions exist between the magnetic Fe ions (the nearest distance between Fe ions is 5.51 Å). The effective magnetic moment is 6.17 μ_B which is lower than the "L-S coupling" moment (6.70 μ_B) calculated for a high-spin Fe(II).[36] Although the overall structures of $BaLn_2FeS_5$[33,37] and $La_4FeSb_2Q_{10}$ are different, both their magnetic properties are merely originated from the corresponding Ba(Ln)/Fe/S(Q) slabs. Detailed comparison reveals that Ba(Ln)/Fe/S(Q) slabs in both structures are similar except that half of the Fe^{2+} centers in $La_4FeSb_2Q_{10}$ are missing (as shown in Figure 4). For example, the intraslab Fe−Fe distances are 5.64, 7.98 Å in $BaLa_2FeS_5$,[33] 5.33, 7.59 Å in $La_4FeSb_2S_{10}$, and 5.51, 7.87 Å in $La_4FeSb_2Se_{10}$, and the interslab Fe−Fe distances are 6.85 Å in $BaLa_2FeS_5$,[33] 6.68 Å in $La_4FeSb_2S_{10}$, and 6.98 Å in $La_4FeSb_2Se_{10}$. Therefore, it may be suggested that the antiferromagnetic interactions existing between the magnetic Fe ions in $La_4FeSb_2Q_{10}$ are parallel to the c-axis as similar as those indicated by the neutron diffraction data of $BaLn_2FeS_5$.[33,37]

(26) Choi, K. -S.; Kanatzidis, M. G. *Inorg. Chem.* **2000**, *39*, 5655–5662.
(27) Odink, D. A.; Carteaux, V.; Payen, C.; Ouvrard, G. *Chem. Mater.* **1993**, *5*, 237–240.
(28) Mauricot, R.; Gressier, P.; Evain, M.; Brec, R. *J. Alloys Compd.* **1995**, *223*, 130–138.
(29) Sleight, A. W.; Prewitt, C. T. *Inorg. Chem.* **1968**, *7*, 2282–2288.
(30) Gulay, L. D.; Olekseyuk, I. D. *J. Alloys Compd.* **2005**, *388*, 274–278.
(31) Jumas, J. C.; Philippot, E.; Maurin, M. *Acta Crystallogr., Sect. B* **1977**, *33*, 3850–3854.
(32) Brockway, L. O. *Kristallografiya* **1934**, *89*, 434–441.
(33) Wakeshima, M.; Ino, K.; Hinatsu, Y. *Solid State Commun.* **2001**, *120*, 145–148.
(34) Hong, Y.-P.; Steinfink, H. *J. Solid State Chem.* **1972**, *5*, 93–104.
(35) O'Connor, C. J. *Prog. Inorg. Chem.* **1982**, *29*, 203–283.
(36) West, A. R. *Solid State Chemistry and Its Applications*; John Wiley & Sons: Chichester, U.K., 1984.
(37) (a) Wakeshima, M.; Hinatsu, Y.; Oikawa, K.; Shimojo, Y.; Morii, Y. *J. Mater. Chem.* **2000**, *10*, 2183–2185. (b) Wakeshima, M.; Hinatsu, Y.; Ishii, Y.; Shimojo, Y.; Morii, Y. *J. Mater. Chem.* **2002**, *12*, 631–634. (c) Wakeshima, M.; Ino, K.; Hinatsu, Y.; Ishii, Y. *Bull. Chem. Soc. Jpn.* **2003**, *76*, 1519–1525.

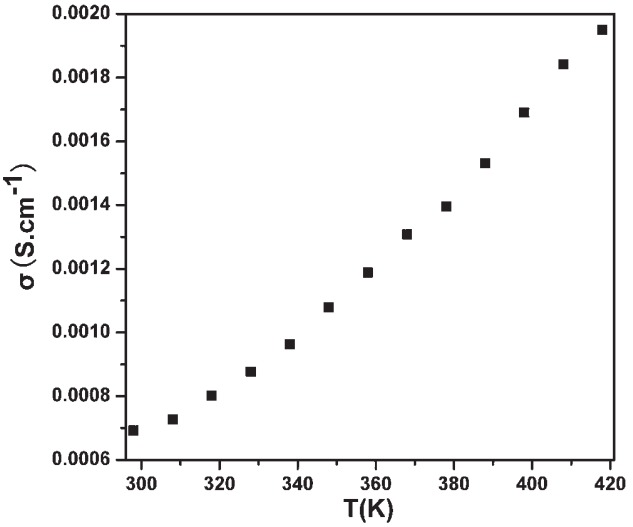

Figure 5. Electrical conductivity temperature dependence of $La_4FeSb_2Se_{10}$.

Optical Properties. The optical band gaps have been measured by the diffuse-reflectance spectra at room temperature. The band gaps were estimated to be 1.00 eV for $La_4FeSb_2S_{10}$ and 0.85 eV for $La_4FeSb_2Se_{10}$ as shown in the Supporting Information. These values are smaller than those of $K_2La_2Sb_2S_9$ (2.20 eV) and $K_2Gd_2Sb_2Se_9$ (1.33 eV).[10] In comparison to K, Fe is less electropositive and is capable of forming stronger covalent interactions with the anionic framework, which may be responsible for the decrease of the band gaps.

Electrical Conductivity. The electrical conductivity−temperature dependence for $La_4FeSb_2Se_{10}$ is shown in Figure 5. The electrical conductivity increases with the temperature increase, which is in accordance with a semiconductor behavior. At 298 K, the electrical conductivity is about 6.9×10^{-4} S/cm for $La_4FeSb_2Se_{10}$ and 4.3×10^{-4} S/cm for $La_4FeSb_2S_{10}$. Because of the chemical reaction between $La_4FeSb_2S_{10}$ and the silver paint above 320 K, the electrical conductivity temperature dependence of $La_4FeSb_2S_{10}$ cannot be measured by this method.

Electronic Structure. To understand the distribution of the orbitals near the Fermi level, the density of states of $La_4FeSb_2Q_{10}$ were calculated and are shown in Figure 6, in which the contribution of La 4f orbitals are not shown. The valence band (VB) is dominated by Q p and Fe 3d block with the minor contributions from Sb 5p, La 5d, whereas the conduction band (CB) are primarily Fe 3d and La 5d orbitals which are hybridized with Sb 5p and Q p orbitals. Below the Fermi level, S 3p and Fe 3d states have strong hybridizations. Above the Fermi level, the contributions from Sb 5p and La 5d states are very weak in comparison to that from Fe 3d. (Supporting Information, Figure S4, 5) The computational direct band gap of $La_4FeSb_2S_{10}$ is 0.90 eV (Supporting Information, Figure S6). The electronic absorption responsible for the optical gap is likely an electronic transfer excitation from S 3p orbitals to Fe 3d orbitals. Similarly, $La_4FeSb_2Se_{10}$ is also a direct band gap semiconductor, and has a band gap of 0.73 eV (Supporting Information, Figure S6). These values are slightly lower than the experimental optical band (Supporting Information, Figure S3), which may be related to the fact that the DFT method usually underestimates the band gap. As band

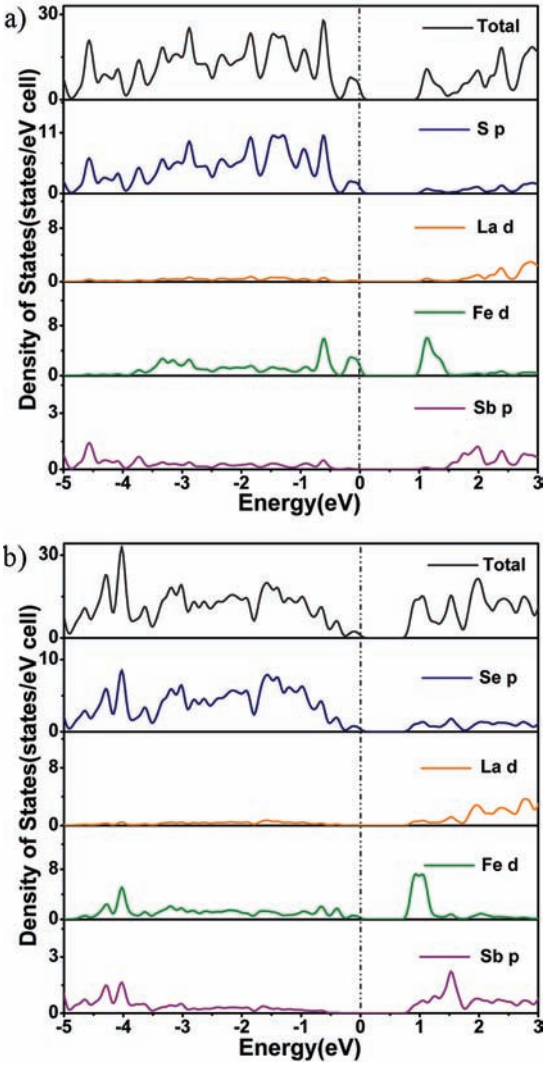

Figure 6. Total and partial densities of states of (a) $La_4FeSb_2S_{10}$ and (b) $La_4FeSb_2Se_{10}$.

structure analyses described above, the band gap is almost determined by the energies of Q-p and (Fe-3d + Sb-5p + La-5d) orbitals. As the energy sequence of p orbitals is 3p(S) < 4p(Se), therefore, the band gap for $La_4FeSb_2Se_{10}$ is smaller than that of $La_4FeSb_2S_{10}$. Such a decrease trend agrees with the experimental measurements described above. A similar chalcogen-originated band gap-decrease has also been observed in Sb_2S_3 (between 1.95 and 2.20 eV) and Sb_2Se_3 (1.11 eV).[38] Compared to the calculated band gap of 1.55 eV for $La_7Sb_9S_{24}$,[5] $La_4FeSb_2S_{10}$ has a smaller band gap of 0.90 eV, which may be because the Fe atoms contribute near the Fermi level.

To gain insight into the characteristics of the Sb−S interactions, the COHP have been investigated. The −COHP curves of Sb(2)−S bonds are shown in Figure 7 as an example. The bonding states of the shortest Sb2−S1 bond (2.46 Å) extends from −6 to −1 eV, these of the slightly longer Sb2−S2 bond (2.55 Å) stretch from −6 to −3 eV. As the lengths of the Sb2−S bond increase, the antibonding characteristic becomes more and more

(38) (a) Fujita, T.; Kurita, K.; Tokiyama, K.; Oda, T. *J. Phys. Soc. Jpn.* **1987**, *56*, 3734–3739. (b) Wood, C.; Shaffer, J. C.; Proctor, W. G. *Phys. Rev. Lett.* **1972**, *29*, 485–487.

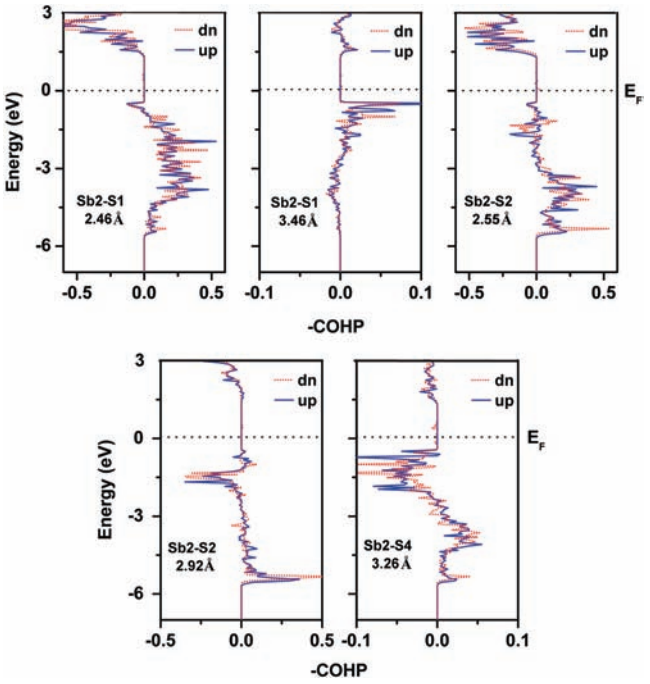

Figure 7. Selected crystal orbital Hamilton population curves of $La_4FeSb_2S_{10}$.

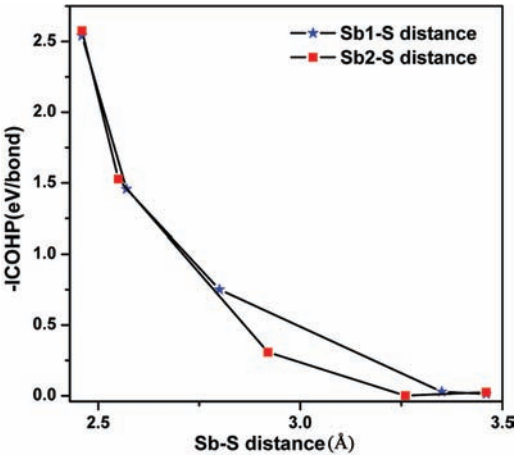

Figure 8. -ICOHP plotted against Sb−S distance.

noticeable. As shown in Table 5 and Figure 8, the integrated COHP (ICOHP) value of the shortest Sb2−S1 bond (2.46 Å) is of 2.54 eV/bond. Those of Sb−S bonds longer than 3.26 Å are below 0.025 eV/bond, that is, only 1% of that of the strongest one. The ICOHP values suggest that the short Sb−S bonds (< 2.57 Å) are much stronger than the longer ones (> 3.26 Å) and the medium Sb−S bonds (2.80 and 2.92 Å) process significant bonding interaction characteristic, which confirm that the local geometries around Sb atoms are indeed 4-fold coordinated incomplete octahedra as revealed by the crystallographic analyses. These data support that the SbQ_4 polyhedra are indeed extending in a novel teeter-totter chain motif as shown in Figure 3.

Conclusion

Two new quaternary chalcogenides $La_4FeSb_2S_{10}$ and $La_4FeSb_2Se_{10}$ have been synthesized and characterized. They exhibit a novel complicated three-dimensional network (Figure 2) constructed by La/Sb/Q (Figure 3) and La/Fe/Q (Figure 4) slabs. The teeter-totter chains of 4-fold coordinated SbQ_4 incomplete octahedra are unique. Both compounds display antiferromagnetic interactions between Fe(II) centers with effective magnetic moments of 5.25 μ_B for $La_4FeSb_2S_{10}$ and 6.17 μ_B for $La_4FeSb_2Se_{10}$, which suggest a high-spin state of Fe(II) with an unquenched orbital moment.

At room temperature, their electrical conductivitie are about 10^{-4} S/cm which are too small for room temperature thermoelectric applications. The optical band gaps are 1.00 eV for $La_4FeSb_2S_{10}$ and 0.85 eV for $La_4FeSb_2Se_{10}$, respectively. The band gap decrease from sulfide to selenide is mainly because the energy increases from 3p (S) to 4p (Se). The VBs of both compounds are dominated by p (Q) and 3d (Fe) orbitals and CBs, 3d (Fe) blocks. The contribution of Fe near the Fermi level narrows the band gap of quaternary $La_4FeSb_2S_{10}$ with respect to ternary $La_7Sb_9S_{24}$. Further explorations on new compounds with a narrower band gap in Ln/M/Sb/Q systems by enhancing the covalent bonding interactions between M and the La/Sb/S slabs are worth pursuing.

Acknowledgment. The research was supported by the National Natural Science Foundation of China under Projects (20773130, 20733003, 20821061, 20973175, 90922021), "Key Project from Fujian Institute of Research on the Structure of Matter" (SZD08002), the "Key Project from Chinese Academy of Sciences" (KJCX2-YW-H20, CXJJ-219), and the Major Programs of Science and Technology Foundation of Fujian Province (2007HZ0005-3).

Supporting Information Available: Two X-ray crystallographic files (CIF) and six figures depicting the local coordination environments of La and Sb atoms, inverse magnetic susceptivities plotted against temperature, UV−vis diffuse reflectance and band structure. This material is available free of charge via the Internet at http://pubs.acs.org.